

# Study of European Cold Streams per 2.24 years: Based on Quantum Gravity Theory with Ultimate Acceleration

Huaiyang Cui

Department of Physics, Beihang University, Beijing, 102206, China

Email: hycui@buaa.edu.cn

(November 8, 2022, submitted to viXra)

**Abstract:** In analogy with the ultimate speed  $c$ , there is an ultimate acceleration  $\beta$ , nobody's acceleration can exceed this limit  $\beta$ , in the solar system,  $\beta=2.961520e+10(m/s^2)$ . Because this ultimate acceleration is large, any effect related to  $\beta$  will become easy to test, including quantum gravity tests. In this paper, an approach is put forward to connect the ultimate acceleration with quantum theory, therefore the ultimate acceleration has quantum effects. At the first, this approach is applied to sunspot problems, the sunspot cycle is calculated to be 10.93 years. Next, this approach is applied to the atmospheric circulations and European climate pattern. Constructive interference condition takes place at three latitudes on the northern hemisphere, that control overall wind fields around the earth. This quantum effect indicates that Europe suffers to a gust of cold streams from arctic regions per 2.24 years, this prediction agrees well with the observed cycles of the quasi-biennial oscillation in the equatorial lower stratosphere. The European climate pattern is under control of the four seasons and the cold streams per 2.24 years.

## 1. Introduction

In general, some quantum gravity proposals [1,2] are extremely hard to test in practice, as quantum gravitational effects are appreciable only at the Planck scale [3]. But ultimate acceleration provides another scheme to deal with quantum gravity effects.

In analogy with the ultimate speed  $c$ , there is an ultimate acceleration  $\beta$ , nobody's acceleration can exceed this limit  $\beta$ , in the solar system,  $\beta=2.961520e+10(m/s^2)$ . Because this ultimate acceleration is large, any effect related to  $\beta$  will become easy to test, including quantum gravity tests. In this paper, an approach is put forward to connect the ultimate acceleration with quantum theory, therefore the ultimate acceleration has quantum effects. At the first, this approach is applied to sunspot problems; next, it is applied to the atmospheric circulations and European climate pattern.

## 2. How to connect the ultimate acceleration with quantum theory

In relativity, the speed of light  $c$  is the ultimate speed, nobody's speed can exceed this limit  $c$ . The relativistic velocity  $u$  of a particle in the coordinate system  $(x_1, x_2, x_3, x_4=ict)$  satisfies

$$u_1^2 + u_2^2 + u_3^2 + u_4^2 = -c^2 . \quad (1)$$

No matter what particles (electrons, molecules, neutrons, quarks), their 4-vector velocities all

have the same magnitude:  $|u|=ic$ . All particles gain **equality** because of the same magnitude of the 4-velocity  $u$ . The acceleration  $a$  of a particle is given by

$$a_1^2 + a_2^2 + a_3^2 = a^2; \quad (a_4 = 0; \quad \because x_4 = ict) \quad (2)$$

Assume that particles have an ultimate acceleration  $\beta$  as the limit, no particle can exceed this acceleration limit  $\beta$ . Subtracting both sides of the above equation by  $\beta^2$ , we have

$$a_1^2 + a_2^2 + a_3^2 - \beta^2 = a^2 - \beta^2; \quad a_4 = 0 \quad (3)$$

It can be rewritten as

$$[a_1^2 + a_2^2 + a_3^2 + 0 + (i\beta)^2] \frac{1}{1 - a^2 / \beta^2} = -\beta^2 \quad (4)$$

Now, the particle has an acceleration whose five components are specified by

$$\alpha_1 = \frac{a_1}{\sqrt{1 - a^2 / \beta^2}}; \quad \alpha_2 = \frac{a_2}{\sqrt{1 - a^2 / \beta^2}}; \quad (5)$$

$$\alpha_3 = \frac{a_3}{\sqrt{1 - a^2 / \beta^2}}; \quad \alpha_4 = 0; \quad \alpha_5 = \frac{i\beta}{\sqrt{1 - a^2 / \beta^2}};$$

where  $\alpha_5$  is the newly defined acceleration in five-dimensional space-time  $(x_1, x_2, x_3, x_4=ict, x_5)$ . Thus, we have

$$\alpha_1^2 + \alpha_2^2 + \alpha_3^2 + \alpha_4^2 + \alpha_5^2 = -\beta^2; \quad \alpha_4 = 0 \quad (6)$$

It means that the magnitude of the newly defined acceleration  $\alpha$  for every particle takes the same value:  $|\alpha|=i\beta$  (constant imaginary number), all particle accelerations gain **equality** for the sake of the same magnitude.

How do resolve the velocity  $u$  and acceleration  $\alpha$  into  $x$ ,  $y$ , and  $z$  components? In a realistic world, a hand can rotate a ball moving around a circular path at constant speed  $v$  with constant centripetal acceleration  $a$ , as shown in Fig.1(a). Likewise, the  $u$  and  $\alpha$  let the particle move spirally, as shown in Fig.1(b), projecting out the real  $x$ ,  $y$ , and  $z$  components.

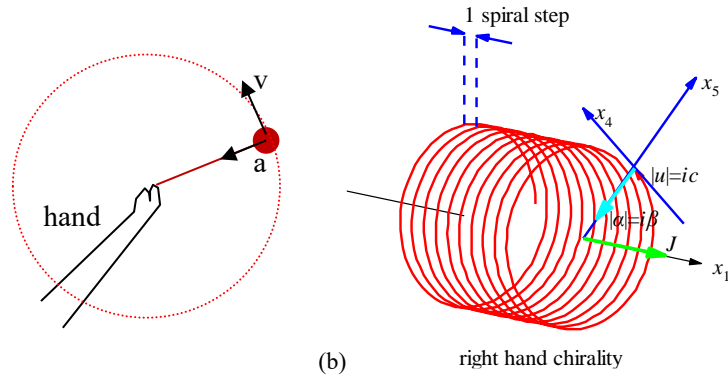


Fig.1 (a) A hand rotates a ball moving around a circular path at constant speed  $v$  with constant centripetal acceleration  $a$ . (b) The particle moves along the  $x_1$  axis with the constant speed  $|u|=ic$  in  $u$  direction and constant centripetal force in the  $x_5$  axis at the radius  $iR$  (imaginary number).

```
<Clet2020 Script>/[26]
double D[100],S[2000];int i,j,R,X,N;
int main(){R=50;X=50;N=600;D[0]=-50;D[1]=0;D[2]=0;D[3]=X;D[4]=0;D[5]=0;D[6]=-50;D[7]=R;D[8]=0;
D[9]=600;D[10]=10;D[11]=R;D[12]=0;D[13]=3645;
Lattice(SPIRAL,D,S);SetViewAngle(0,80,-50);DrawFrame(FRAME_NULL,1,0xfffff);
Draw("LINE,0,2,XYZ,0","-150,0,0,-50,0,0");Draw("ARROW,0,2,XYZ,10","50,0,0,150,0,0");
SetPen(2,0xffff0000);Plot("POLYLINE,0,600,XYZ",S[9];i=9+3*N-6;Draw("ARROW,0,2,XYZ,10",S[i]);
```

```

TextHang(S[i],S[i+1],S[i+2]," #if|u|=ic#t");TextHang(150,0,0," #ifx#sd1#t");SetPen(2,0x005fff);
Draw("LINE,1,2,XYZ,8",-50,0,50,-50,0,100");Draw("LINE,1,2,XYZ,8",-40,0,50,-40,0,100");
Draw("ARROW,0,2,XYZ,10",-80,0,100,-50,0,100");Draw("ARROW,0,2,XYZ,10",-10,0,100,-40,0,100");
TextHang(-50,0,110,"1 spiral step");i=9+3*N;S[i]=50;S[i+1]=10;S[i+2]=10;
Draw("ARROW,0,2,XYZ,10",50,0,0,50,80,80);TextHang(50,80,80," #ifx#sd5#t");
Draw("ARROW,0,2,XYZ,10",50,72,0,50,0,72);TextHang(50,0,72," #ifx#sd4#t");
SetPen(3,0x00ffff);Draw("ARROW,0,2,XYZ,15",S[i-3]);TextHang(S[i],S[i+1],S[i+2]," #if|α|=iβ#t");
SetPen(3,0x00ff00);Draw("ARROW,0,2,XYZ,15",50,0,0,120,0,0);TextHang(110,5,5," #ifj#t");
TextHang(-60,0,-80," right hand chirality");#v07=?>A#t

```

In analogy with the ball in a circular path, consider a particle in one-dimensional motion along the  $x_l$  axis at the speed  $v$ , in Fig.1(b) it moves with the constant speed  $|u|=ic$  almost along the  $x_d$  axis and slightly along the  $x_l$  axis, and the constant centripetal acceleration  $|\alpha|=i\beta$  in the  $x_5$  axis at the constant radius  $iR$  (imaginary number); the coordinate system  $(x_l, x_d=ict, x_5=iR)$  establishes a cylinder coordinate system in which this particle moves spirally at the speed  $v$  along the  $x_l$  axis. According to the usual centripetal acceleration formula  $a=v^2/r$ , the acceleration in the  $x_d$ - $x_5$  plane is given by

$$a = \frac{v^2}{r} \Rightarrow i\beta = \frac{|u|^2}{iR} = -\frac{c^2}{iR} = i\frac{c^2}{R} \quad (7)$$

Therefore, the track of the particle in the cylinder coordinate system  $(x_l, x_d=ict, x_5=iR)$  forms a shape, called **acceleration-roll**. The faster the particle moves along the  $x_l$  axis, the longer the spiral step is.

Like a steel spring that contains an elastic wave, the track in the acceleration-roll in Fig.1(b) can be described by a wave function whose phase changes  $2\pi$  for one spiral step. Apparently, **this wave is just the de Broglie's matter wave for electrons, protons or quarks, etc.**

**Theorem:** the acceleration-roll bears matter wave.

$$\psi = \exp\left(i\frac{\beta}{c^3} \int_0^x (u_1 dx_1 + u_2 dx_2 + u_3 dx_3 + u_4 dx_4)\right) \quad (8)$$

**Proof:** See ref. [28,30].

Depending on the particle under investigation, this wave function may have different explanations. If the  $\beta$  is replaced by the Planck constant, the wave function of electrons is given by

$$\text{assume: } \beta = \frac{mc^3}{\hbar} \quad (9)$$

$$\psi = \exp\left(\frac{i}{\hbar} \int_0^x (mu_1 dx_1 + mu_2 dx_2 + mu_3 dx_3 + mu_4 dx_4)\right)$$

where  $mu_4 dx_4 = -Edt$ , it strongly suggests that the wave function is just the de Broglie's matter wave [4,5,6].

Considering another explanation to  $\psi$  for planets in the solar system, no Planck constant can be involved. But, in a many-body system with the total mass  $M$ , the data analysis [28] tells us that the ultimate acceleration can be rewritten in terms of **Planck-constant-like constant  $h$**  as

$$\text{assume: } \beta = \frac{c^3}{hM} \quad (10)$$

$$\psi = \exp\left(\frac{i}{hM} \int_0^x (u_1 dx_1 + u_2 dx_2 + u_3 dx_3 + u_4 dx_4)\right)$$

The constant  $h$  will be determined by experimental observations. This paper will show that this wave function is applicable to several many-body systems in the solar system, the wave function is called the **acceleration-roll wave**.

Tip: actually, ones cannot get to see the acceleration-roll of a particle in the relativistic space-time ( $x_1, x_2, x_3, x_4 = ict$ ) ; only get to see it in the cylinder coordinate system ( $x_1, x_4 = ict, x_5 = iR$ ).

### 3. How to determine the ultimate acceleration

In Bohr's orbit model for planets or satellites, as shown in Fig.2, the circular quantization condition is given in terms of relativistic matter wave in gravity by

$$\left. \begin{aligned} \frac{\beta}{c^3} \oint_L v_l dl = 2\pi n \\ v_l = \sqrt{\frac{GM}{r}} \end{aligned} \right\} \Rightarrow \sqrt{r} = \frac{c^3}{\beta \sqrt{GM}} n; \quad n = 0, 1, 2, \dots \quad (11)$$

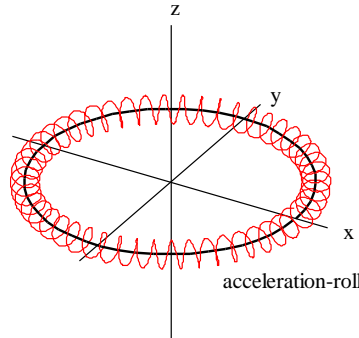


Fig.2 A planet 2D orbit around the sun, an acceleration-roll winding around the planet.

```
<Clet2020 Script>[[26]
int i,j,k; double r,rot,x,y,z,D[20],F[20],S[200]; int main(){SetViewAngle("temp0,theta60,phi-30");
DrawFrame(FRAME LINE,1,0xafffaf);r=80;Spiral(); TextHang(r,-r,0,"acceleration-roll");
r=110;TextHang(r,0,0,"x");TextHang(0,r,0,"y");TextHang(0,0,r,"z");}
Spiral(){r=80;j=10;rot=j/r;k=2*PI/rot+1;
for(i=0;i<k;i+=1){D[0]=x;D[1]=y;D[2]=z;D[6]=x;D[7]=y;D[8]=r;
x=r*cos(rot*i);y=r*sin(rot*i);z=0;if(i==0) continue;
SetPen(2,0x00);F[0]=D[0];F[1]=D[1];F[2]=x;F[3]=y;Draw("LINE,0,2,XY","F");SetPen(1,0xff0000);
D[3]=x;D[4]=y;D[5]=z; D[9]=40;D[10]=10;D[11]=8;D[12]=0;D[13]=360;
Lattice(SPIRAL,D,S);Plot("POLYLINE,0,40,XYZ",S[9]);}
}#v07=?>A#
```

The solar system, Jupiter's satellites, Saturn's satellites, Uranus' satellites, and Neptune's satellites as five different many-body systems are investigated with the Bohr's orbit model. After fitting observational data as shown in Fig.3, their ultimate accelerations are obtained in Table 1. The predicted quantization blue-lines in Fig.3(a), Fig.3(b), Fig.3(c), Fig.3(d) and Fig.3(e) agree well with experimental observations for those *inner constituent planets or satellites*.

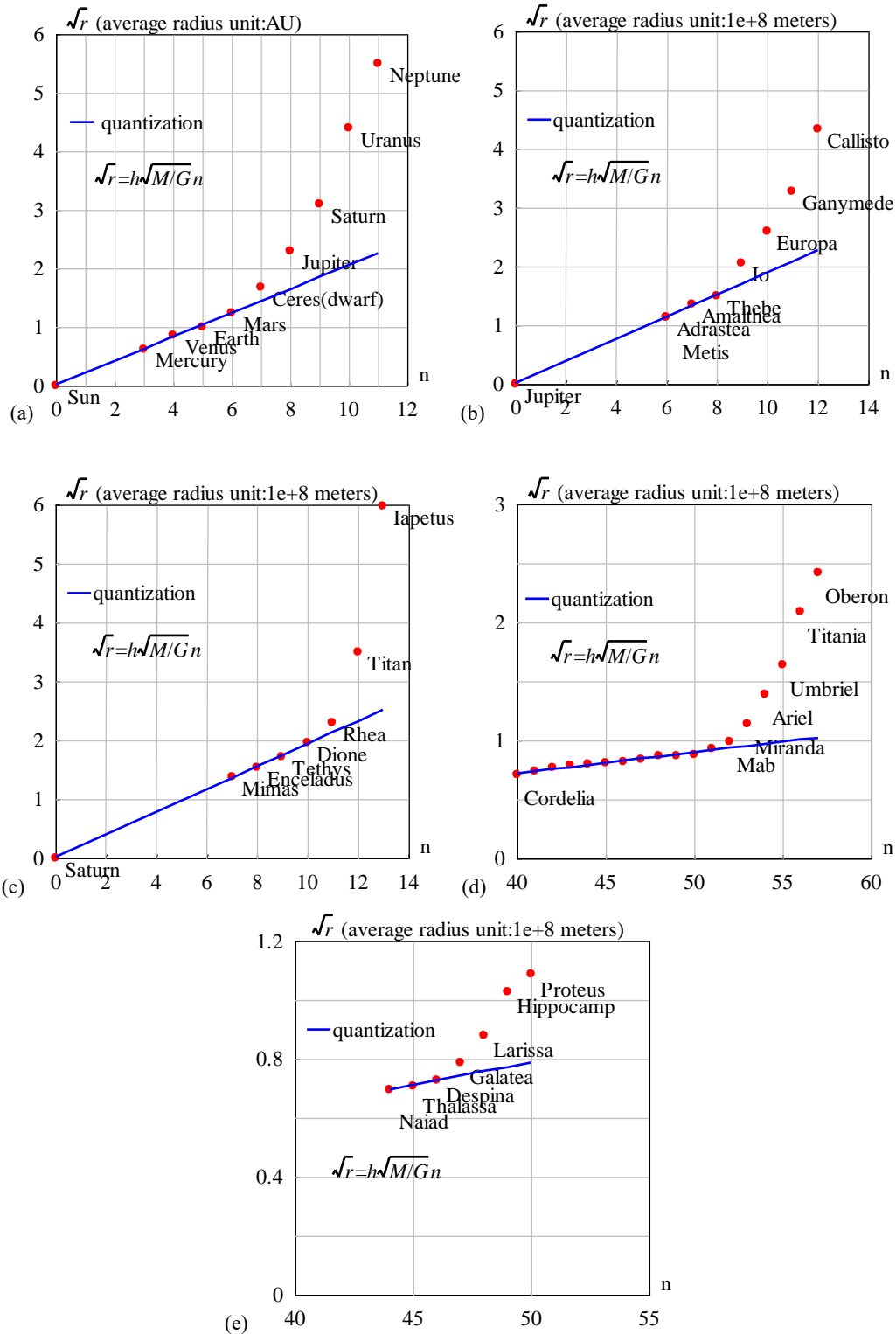


Fig.3 The orbital radii are quantized for inner constituents. (a) the solar system with  $h=4.574635e-16$  ( $m^2s^{-1}kg^{-1}$ ). The relative error is less than 3.9%. (b) the Jupiter system with  $h=3.531903e-16$  ( $m^2s^{-1}kg^{-1}$ ). Metis and Adrastea are assigned the same quantum number for their almost same radius. The relative error is less than 1.9%. (c) the Saturn system with  $h=6.610920e-16$  ( $m^2s^{-1}kg^{-1}$ ). The relative error is less than 1.1%. (d) the Uranus system with  $h=1.567124e-16$  ( $m^2s^{-1}kg^{-1}$ ).  $n=0$  is assigned to Uranus. The relative error is less than 2.5%. (e) the Neptune system with  $h=1.277170e-16$  ( $m^2s^{-1}kg^{-1}$ ).  $n=0$  is assigned to Neptune. The relative error is less than 0.17%.

Table 1 Planck-constant-like constant  $h$ ,  $N$  is constituent particle number with smaller orbital inclination.

system	$N$	$M/M_{\text{earth}}$	$\beta$ (m/s <sup>2</sup> )	$h$ (m <sup>2</sup> s <sup>-1</sup> kg <sup>-1</sup> )	Prediction
Solar planets	9	333000	2.961520e+10	4.574635e-16	Fig.3(a)
Jupiter' satellites	7	318	4.016793e+13	3.531903e-16	Fig.3(b)
Saturn's satellites	7	95	7.183397e+13	6.610920e-16	Fig.3(c)
Uranus' satellites	18	14.5	1.985382e+15	1.567124e-16	Fig.3(d)
Neptune 's satellites	7	17	2.077868e+15	1.277170e-16	Fig.3(e)

Besides every  $\beta$ , our interest shifts to the constant  $h$  in Table 1, which is defined as

$$h = \frac{c^3}{M\beta} \Rightarrow \sqrt{r} = h\sqrt{\frac{M}{G}}n \quad (12)$$

In a many-body system with a total mass of  $M$ , a constituent particle has the mass of  $m$  and moves at the speed of  $v$ , it is easy to find that the wavelength of de Broglie's matter wave should be modified for planets and satellites as

$$\lambda_{de\_Broglie} = \frac{2\pi\hbar}{mv} \Rightarrow \text{modify} \Rightarrow \lambda = \frac{2\pi hM}{v} \quad (13)$$

where  $h$  is a **Planck-constant-like constant**. Usually, the total mass  $M$  is approximately equal to the central-star's mass. It is found that this modified matter wave works for quantizing orbits correctly in Fig.3 [28,29]. The key point is that the various systems have almost the same Planck-constant-like constant  $h$  in Table 1 with a mean value of  $3.51\text{e-}16 \text{ m}^2\text{s}^{-1}\text{kg}^{-1}$ , at least having the same magnitude! The acceleration-roll wave is a generalized matter wave on a planetary scale.

In Fig.3(a), the blue straight line expresses the linear regression relation among the Sun, Mercury, Venus, Earth and Mars, their quantization parameters are  $hM=9.098031\text{e+}14(\text{m}^2/\text{s})$ . The ultimate acceleration is fitted out to be  $\beta=2.961520\text{e+}10 \text{ (m/s}^2\text{)}$ . Where,  $n=3,4,5,\dots$  were assigned to solar planets, the sun was assigned a quantum number  $n=0$  because the sun is in the **central state**.

#### 4. Optical model of the central state

The acceleration-roll wave as the relativistic matter wave generalized in gravity is given by

$$\psi = \exp\left(\frac{i}{hM} \int_0^x v_l dl\right); \quad \lambda = \frac{2\pi hM}{v_l} = \frac{2\pi c^3}{v_l \beta} \quad (14)$$

In a central state  $n=0$ , if the coherent length of the acceleration-roll wave is long enough, its head may overlap with its tail when the particle moves in a closed orbit in space-time, as shown in Fig.4(a), the interference of the acceleration-roll wave between its head and tail will occur in the overlapping zone. The overlapped wave is given by

$$\psi(r) = 1 + e^{i\delta} + e^{i2\delta} + \dots + e^{i(N-1)\delta} = \frac{1 - \exp(iN\delta)}{1 - \exp(i\delta)} \quad (15)$$

$$\delta(r) = \frac{1}{hM} \oint_L (v_l) dl = \frac{2\pi\omega r^2}{hM} = \frac{2\pi\beta\omega r^2}{c^3}$$

where  $N$  is the overlapping number which is determined by the coherent length of the acceleration-roll wave,  $\delta$  is the phase difference after one orbital motion,  $\omega$  is the angular speed of the solar rotation. The above equation is a multi-slit interference formula in optics, for a larger  $N$  it is called the Fabry-Perot interference formula.

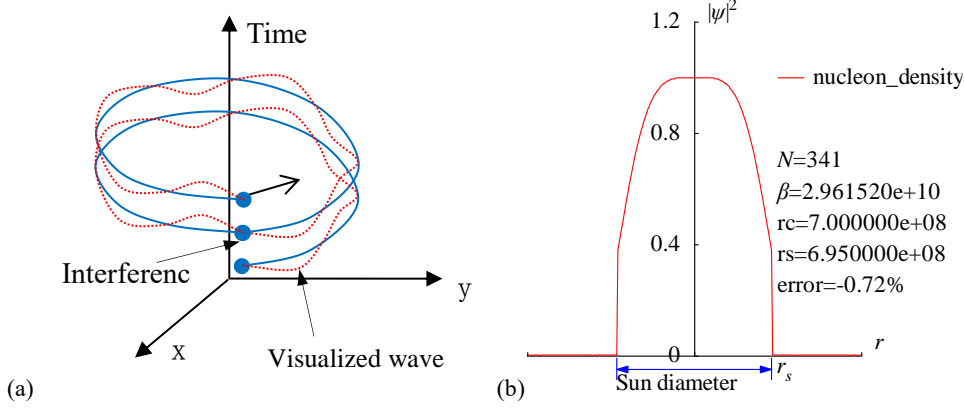


Fig.4 (a)The head of the acceleration-roll wave may overlap with its tail. (b) The matter distribution  $|\psi|^2$  around the Sun has been calculated in the radius direction.

```
<Clet2020 Script>[/[26]
int i,j,k,m,n,N,nP[10];
double beta,H,B,M,r_r_unit,x,y,z,delta,D[1000],S[1000],a,b,rs,rc,rot,atm_height; char str[100];
main(){k=150;rs=6.95e8;rc=0;x=25.05;rot=2*PI/(x*24*3600);n=0; N=341;
beta=2.961520e10;H=SPEEDC*SPEEDC*SPEEDC/beta;M=1.9891E30; atm_height=2e6; r_unit=1E7;
b=PI/(2*PI*rot*rs/H);
for(i=-k;i<k;i+=1){r=abs(i)*r_unit;
if(r<rs+atm_height) delta=2*PI*rot*r/H; else delta=2*PI*sqrt(GRAVITYC*M*r)/H;//around the star
y=SumJob("SLIT_ADD,@N,@delta",D); y=y/(N*N);
S[n]=i;S[n+1]=y; if(i>0 && rc==0 && y<0.001) rc=r;D[n]=i;D[n+1]=z;n+=2;}
SetAxis(X_AXIS,-k,0,k,"#if; ;");SetAxis(Y_AXIS,0,0,1.2,"#if|#su2#;0;0.4;0.8;1.2;");
DrawFrame(FRAME_SCALE,1,0xaffaf); z=100*(rs-rc)/rs;
SetPen(1,0xff0000);Polyline(k+k,S,k/2,1,"nucleon_density"); SetPen(1,0x0000ff);//Polyline(k+k,D);
//Draw("LINE,0,2,XY,0","20,0.5,60,0.6");TextHang(60,0.6,0,"core");
r=rs/r_unit;y=-0.05;D[0]=-r;D[1]=y;D[2]=r;D[3]=y; Draw("ARROW,3,2,XY,10,100,10,10,"D);
Format(str,"#ifN#t=#d#n#i#β#t=#e#nrc=#e#nrs=#e#nerror=#.2f%",N,beta,rc,rs,z);
TextHang(k/2,0.7,0,str);TextHang(r+5,y/2,0,"#if#sds#");TextHang(-r,y,0,"Sun diameter");
}#v07=?>A#t
```

The acceleration-roll wave function  $\psi$  needs a further explanation. In quantum mechanics,  $|\psi|^2$  equals to the probability of finding an electron due to Max Burn's explanation; in astrophysics,  $|\psi|^2$  equals to the probability of finding a nucleon (proton or neutron) *averagely on an astronomic scale*, because all mass is mainly made of nucleons, we have

$$|\psi|^2 \propto \text{nucleon\_density} \quad (16)$$

It follows from the multi-slit interference formula that the interference intensity at maxima is proportional to  $N^2$ , that is

$$N^2 = \frac{|\psi(0)_{\text{multi-wavelet}}|^2}{|\psi(0)_{\text{one-wavelet}}|^2} \quad (17)$$

What matter plays the role of “one-wavelet” in the solar core or earth core? We choose air-vapor at the sea level on the earth's surface as the “reference matter: one-wavelet”. Thus, the

overlapping number  $N$  is estimated by

$$N^2 = \frac{|\psi(0)_{multi-wavelet}|^2}{|\psi(0)_{one-wavelet}|^2} \approx \frac{core\_nucleon\_density_{r=0}}{air\_vapor\_density_{r=sea}} \quad (18)$$

Although today there is no air-vapor on the solar surface, does not hinder to select it as the reference matter. The solar core has a maximum density of  $1.5e+5\text{kg/m}^3$  [31], comparing to the air-vapor density of  $1.29\text{kg/m}^3$  at the sea level on the earth, the solar overlapping number  $N$  is calculated as  $N=341$ . The earth's core density is  $5.53e+3\text{kg/m}^3$ , the earth's overlapping number  $N$  is calculated as  $N=65$ .

Sun's angular speed at the equator is known as  $\omega=2\pi/(25.05*24*3600)$ , unit:  $\text{s}^{-1}$ . Its mass  $1.9891e+30$  (kg), radius  $6.95e+8$  (m), mean density  $1408$  ( $\text{kg/m}^3$ ), the solar core has a maximum density of  $1.5e+5\text{kg/m}^3$  [31], the ultimate acceleration  $\beta=2.961520e+10$  ( $\text{m/s}^2$ ), the constant  $hM=9.100745e+14$  ( $\text{m}^2/\text{s}$ ). According to the  $N=341$ , the matter distribution of the  $|\psi|^2$  is calculated in Fig.4(b), it agrees well with the general description of the sun's interior. The radius of the sun is calculated to be  $r=7e+8$  (m) with a relative error of  $0.72\%$  in Fig.4(b), which indicates that the sun radius strongly depends on the sun's self-rotation.

## 5. Earth's central state and space debris distribution

Applying the acceleration-roll wave to the Moon, as illustrated in Fig.5(a), the Moon has been assigned a quantum number of  $n=2$  in the author's early study [28]. According to the quantum condition, the ultimate acceleration is fitted out to be  $\beta=1.377075e+14$  ( $\text{m/s}^2$ ) in the earth system. Another consideration is to take the quasi-satellite's perigee into account, for the moon and 2004\_GU9 etc., as shown in Fig.5(b), but this consideration requires further understanding of its five quasi-satellites [28].

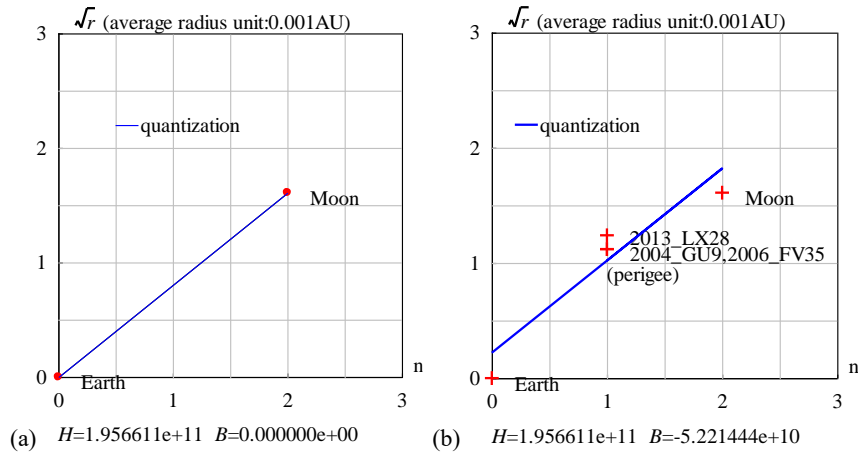


Fig.5 Orbital quantization for moon and quasi-satellites to the Earth,  $H=hM$ .

```
<Clet2020 Script>/[26]
char str[200];int i,j,k,N,nP[10]; double x,y,z,M,r_unit,a,b,B,H,r_ave[20],dP[10],D[1000];
double orbit[10]={0,2.57,0,}; double e[10]={0, 0.0549,0,0,0,0,0,0,0,};
int qn[10]={0,2,3,4,5,6,7,8,9,10,}; char Stars[100]="Earth;Moon;";
int main(){ N=2; M=5.97237E24; r_unit=1.495978707e8;
for(i=0;i<N;i+=1) {x=orbit[i];y=e[i]; z=x*(1+sqrt(1-y*y))/2; r_ave[i]=z;//average_radius
D[i+1]=qn[i];D[i+1+1]=sqrt(z); }
DataJob("REGRESSION,2",D,dP);b=dP[0];a=dP[1];
SetAxis(X_AXIS,0,0,3,"n;0;1;2;3;");
SetAxis(Y_AXIS,0,0,3,"#i#r#t#t (average radius unit:0.001AU);0;1;2;3;");
DrawFrame(0x0166,1,0xaffaf); Polyline(N,D);
SetPen(2,0xff0000); Plot("OVALFILL,0.2,XY,3,3, ",D);
for(i=0;i<N;i+=1) {nP[0]=TAKE;nP[1]=i;TextJob(nP,Stars,str);x=qn[i]+0.2;y=sqrt(orbit[i])-0.05;TextHang(x,y,0,str);}
```

```

x=GRAVITYC*M*r unit;z=sqrt(x);H=z*a;B=-z*b;
TextAt(100,450,"#iH#=#e #iB#=#e",H,B);
for(i=0;i<N;i+=1) {y=b+a*qn[i];D[i]=qn[i];D[i+1]=y;}
SetPen(1,0x0000ff);Polyline(N,D,0.5,2.2,"quantization");//check
} #v07=?>A#t

```

The earth's angular speed is known as  $\omega=2\pi/(24*3600)$ , unit  $s^{-1}$ . Its mass  $5.97237e+24$ (kg), radius  $6.371e+6$ (m), core density  $5530$ (kg/m<sup>3</sup>), the ultimate acceleration  $\beta=1.377075e+14$ (m/s<sup>2</sup>), the constant  $hM=1.956611e+11$ (m<sup>2</sup>/s).

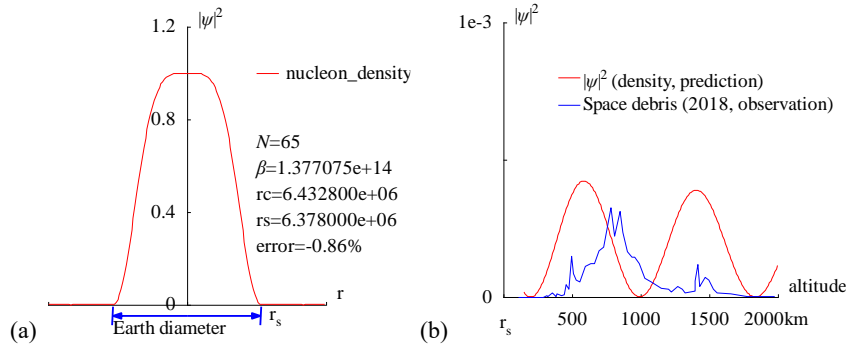
We have estimated that the wave overlapping number in the central state of the earth is  $N=65$ , the matter distribution  $|\psi|^2$  in radius direction is calculated as shown in Fig.6(a), where the self-rotation near its equator has the period of 24 hours:

$$\delta(r) = \frac{1}{hM} \oint_L (v_i) dl = \frac{2\pi r}{hM} \omega r = \frac{2\pi\beta\omega r^2}{c^3} . \quad (19)$$

The matter distribution has a central maximum at the earth's heart, which gradually decreases to zero near the earth surface, then rises the secondary peaks and attenuates down off. The radius of the earth is calculated to be  $r=6.4328e+6$  (m) with a relative error of 0.86% using the interference of its acceleration-roll wave. Space debris over the atmosphere has a complicated evolution [7,8], and has itself speed

$$v_i = \sqrt{\frac{GM}{r}}; \quad \delta(r) = \frac{1}{hM} \oint_L (v_i) dl = \frac{\beta}{c^3} \oint_L (v_i) dl = \frac{2\pi\beta}{c^3} \sqrt{GMr} . \quad (20)$$

The secondary peaks over the atmosphere up to 2000km altitude are calculated in Fig.6(b) which agree well with the space debris observations [16]; the peak near 890 km altitude is due principally to the January 2007 intentional destruction of the FengYun-1C weather spacecraft, while the peak centered at approximately 770 km altitude was created by the February 2009 accidental collision of Iridium 33 (active) and Cosmos 2251 (derelict) communication spacecraft [16,18]. The observations based on the incoherent scattering radar EISCAT ESR located at 78°N in Jul. 2006 and in Oct. 2015 [21,22,23] are respectively shown in Fig.6(c) and (d). This prediction of secondary peaks also agrees well with other space debris observations [24,25].



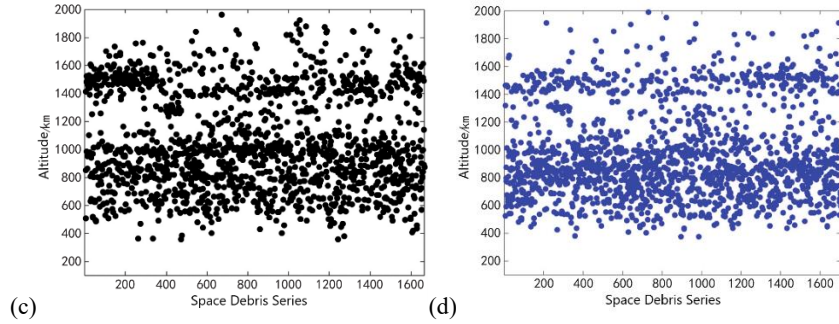


Fig.6 (a) The radius of the Earth is calculated out  $r=6.4328e+6$  (m) with a relative error of 0.86% by the interference of its acceleration-roll wave; (b) The prediction of the space debris distribution up to 2000km altitude; (c) The space debris distribution in Jul. 2006, Joint observation based on the incoherent scattering radar EISCAT ESR located at 78°N [21]; (d) The space debris distribution in Oct. 2015, Joint observation based on the incoherent scattering radar EISCAT ESR located at 78°N [21].

```
<Clet2020 Script>//[26]
int i,j,k,m,n,N,nP[10]; double H,B,M,v_r,r,AU,r_unit,x,y,z,delta,D[10],S[1000];
double rs,rc,rot,a,b,atm_height,beta; char str[100];
main(){k=80;rs=6.378e6;rc=0;atm_height=1.5e5;n=0;N=65;
beta=1.377075e+14;H=SPEEDC*SPEEDC*SPEEDC/beta;
M=5.97237e24;AU=1.496E11;r_unit=1e-6*AU;rot=2*PI/(24*60*60);//angular speed of the Earth
for(i=-k;i<k;i+=1){r=abs(i)*r_unit;
if(r<rs+atm_height)v_r=rot*r;elsev_r=sqrt(GRAVITYC*M*r);//around the Earth
delta=2*PI*v_r/H;y=SumJob("SLIT_ADD,@N,@delta",D);y=y/(N*N);
if(y>1)y=1;S[n]=i;S[n+1]=y;if(i>0&&rc==0&&y<0.001)rc=r;n+=2;}
SetAxis(X_AXIS,-k,0,k,"r; ;");SetAxis(Y_AXIS,0,0,1.2,"#i|ψ|#su2#t;0;0.4;0.8;1.2;");
DrawFrame(FRAME_SCALE,1,0,affaf);x=50;z=100*(rs-rc)/rs;
SetPen(1,0,ff0000);Polyline(k+k,S,k/2,1,"nucleon_density");
r=rs/r_unit;y=-0.05;D[0]=-r;D[1]=y;D[2]=r;D[3]=y;
SetPen(2,0,0000ff);Draw("ARROW,3,2,XY,10,100,10,10,"D);
Format(str,"#iN#t=%d#n#i#t=%e#nrc=%e#nrs=%e#nerror=%.2f%",N,beta,rc,rs,z);
TextHang(k/2,0.7,0,str);TextHang(r+5,y/2,0,"r#sds#t");TextHang(-r,y+y,0,"Earth diameter");
}#v07=?>A#t
```

```
<Clet2020 Script>//[26]
int i,j,k,m,n,N,nP[10]; double H,B,M,v_r,r,AU,r_unit,x,y,z,delta,D[10],S[10000];
double rs,rc,rot,a,b,atm_height,p,T,R1,R2,R3; char str[100]; int
Debris[96]={110,0,237,0,287,0,317,2,320,1,357,5,380,1,387,4,420,2,440,3,454,14,474,9,497,45,507,26,527,19,557,17,597,34,63
4,37,664,37,697,51,727,55,781,98,808,67,851,94,871,71,901,50,938,44,958,44,991,37,1028,21,1078,17,1148,10,1202,9,1225,6,
1268,12,1302,9,1325,5,1395,7,1395,18,1415,36,1429,12,1469,22,1499,19,1529,9,1559,5,1656,4,1779,1,1976,1,};
main(){k=80;rs=6.378e6;rc=0;atm_height=1.5e5;n=0;N=65;
H=1.956611e11;M=5.97237e24;AU=1.496E11;r_unit=1e4;
rot=2*PI/(24*60*60);//angular speed of the Earth
b=PI/(2*PI*rot*rs/H);R1=rs/r_unit;R2=(rs+atm_height)/r_unit;R3=(rs+2e6)/r_unit;
for(i=R2;i<R3;i+=1){r=abs(i)*r_unit;delta=2*PI*sqrt(GRAVITYC*M*r)/H;
y=SumJob("SLIT_ADD,@N,@delta",D);y=1e3*y/(N*N);//visualization scale:1000
if(y>1)y=1;S[n]=i;S[n+1]=y;n+=2;}
SetAxis(X_AXIS,R1,R1,R3,"altitude; r#sds#t;500;1000;1500;2000km ;");
SetAxis(Y_AXIS,0,0,1,"#i|ψ|#su2#t;0; ;1e-3;");DrawFrame(FRAME_SCALE,1,0,affaf);x=R1+(R3-R1)/5;
SetPen(1,0,ff0000);Polyline(n/2,S,x,0.8,"#i|ψ|#su2#t (density, prediction)");
for(i=0;i<48;i+=1){S[i+1]=R1+(R3-R1)*Debris[i+1]/2000;S[i+1+1]=Debris[i+1+1]/300;}
SetPen(1,0,0000ff);Polyline(48,S,x,0.7,"Space debris (2018, observation)");}#v07=?>A#t
```

## 6. Sunspot cycle

The **coherence length** of waves is usually mentioned but the **coherence width** of waves is rarely discussed in quantum mechanics, simply because the latter is not a matter for electrons, nucleon, or photons, but it is a matter in astrophysics. The analysis of observation data tells us that on the planetary scale, the coherence width of acceleration roll waves can be extended to 1000 kilometers or more, as illustrated in Fig.7(a), the overlap may even occur in the width direction, thereby bringing new aspects to wave interference.

In the solar convective zone, adjacent convective arrays form a top-layer flow, a middle-layer gas, and a ground-layer flow, similar to the concept of **molecular current** in

electromagnetism. Considering one convective ring at the equator as shown in Fig.7(b), there is an apparent velocity difference between the top-layer flow and the middle-layer gas, where their acceleration-roll waves are denoted respectively by

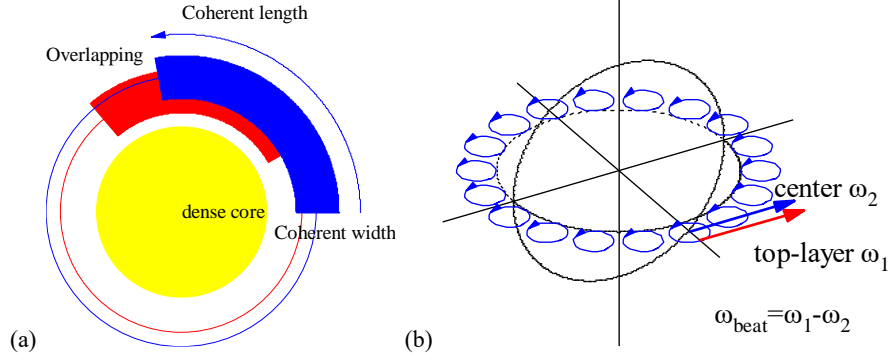


Fig.7 (a) Illustration of overlapping in the coherent width direction. (b) In convective rings at the equator, the speed difference causes a beat frequency.

```
<Clet2020 Script>// [26]
int i, j, k, R, D[500];
main(){DrawFrame(FRAME_NULL,1,0xaffaf);
R=60; SetPen(1,0xffff00);
D[0]=-R; D[1]=-R; D[2]=R; D[3]=R; Draw("ELLIPSE,1,2,XY,0",D);
R=85; k=15; SetPen(1,0xff0000);
D[0]=-R; D[1]=-R; D[2]=R; D[3]=R; Draw("ELLIPSE,0,2,XY,0",D);
D[0]=0; D[1]=0; D[2]=R-k; D[3]=0; D[4]=R+k;D[5]=0;
Draw("SECTOR,1,3,XY,15,30,130,0",D);
R=95; k=15; SetPen(1,0x00ff);
D[0]=-R; D[1]=-R; D[2]=R; D[3]=R; Draw("ELLIPSE,0,2,XY,0",D);
D[0]=0; D[1]=0; D[2]=R-k; D[3]=0; D[4]=R+k;D[5]=0;
Draw("SECTOR,1,3,XY,15,0,100,0",D);D[4]=R+k+k;
Draw("SECTOR,3,3,XY,15,0,100,0",D);
TextHang(0,0,0,"dense core");TextHang(R-k-k,-k,0,"Coherent width");
TextHang(0,R+k+k+k,0,"Coherent length");TextHang(-R,R+k,0,"Overlapping");
}#v07=?>A#t
```

```
<Clet2020 Script>//Clet is a C compiler[26]
double beta,H,M,N,dP[20],D[2000],r,rs,rot,x,y,v1,v2,K1,K2,T1,T2,T,Lamda,L; int i,j,k;
int main(){beta=2.961520e10; H=SPEEDC*SPEEDC*SPEEDC/beta;
M=1.9891E30; rs=6.95e8;rot=2*PI/(25.05*24*3600);v1=rot*rs;K1=v1*v1/2;//T1=2*PI*H/K1;
v2=6100;//0.7346*sqrt(BOLTZMANN*5700/MP)+0.2485*sqrt(BOLTZMANN*5700/(MP+MP));
K2=v2*v2/2;T2=2*PI*H/(K2-K1);T=T2/24*3600*365.2422;
Lamda=2*PI*H/(v2-v1);L=2*PI*rs/Lamda;
SetViewAngle("temp0,theta60,phi-60");
DrawFrame(FRAME_LINE,1,0xaffaf);Overlook("2,1,60", D);
TextAt(10,10,"v1=%d, v2=%d, T=%f y, #n λ=%e, L=%f",v1,v2,T, Lamda,L);
SetPen(1,0x4f4fff); for(i=0;i<18;i+=1) {v1=i*2*PI/18; x=70*cos(v1);y=70*sin(v1);Ring(i);
SetPen(2,0xff0000);Draw("ARROW,0,2,XYZ,15","80,0,0,80,60,0");
TextHang(100,20,0,"top-layer ω#sd1#t"); SetPen(2,0x0000ff);
Draw("ARROW,0,2,XYZ,15","70,0,0,70,60,0");
TextHang(50,60,0,"center ω#sd2#t");TextHang(140,-30,0," ω#sdbeat#t=ω#sd1#t-ω#sd2#t");
}
Ring(){ k=0;N=20; r=10;
for(j=0;j<N+2;j+=1) {k=j+j+j; v2=j*2*PI/N;
D[k]=x+r*cos(v2);D[k+1]=y+r*sin(v2); D[k+2]=0;}
Plot("POLYLINE,4,22,XYZ,8",D);
}#v07=?>A
```

$$\begin{aligned} \psi &= \psi_{top} + C\psi_{middle} \\ \psi_{top} &= \exp\left[\frac{i\beta}{c^3} \int_L (v_1 dl + \frac{-c^2}{\sqrt{1-v_1^2/c^2}} dt)\right] \\ \psi_{middle} &= \exp\left[\frac{i\beta}{c^3} \int_L (v_2 dl + \frac{-c^2}{\sqrt{1-v_2^2/c^2}} dt)\right] \end{aligned} \quad (21)$$

Their interference in the coherent width direction leads to a beat phenomenon

$$|\psi|^2 = |\psi_{top} + C\psi_{middle}|^2 = 1 + C^2 + 2C \cos\left[\frac{2\pi}{\lambda_{beat}} \int_L dl - \frac{2\pi}{T_{beat}} t\right]$$

$$\frac{2\pi}{T_{beat}} = \frac{\beta}{c^3} \left( \frac{c^2}{\sqrt{1-v_1^2/c^2}} - \frac{c^2}{\sqrt{1-v_2^2/c^2}} \right) \approx \frac{\beta}{c^3} \left( \frac{v_1^2}{2} - \frac{v_2^2}{2} \right) \quad (22)$$

$$\frac{2\pi}{\lambda_{beat}} = \frac{\beta}{c^3} (v_1 - v_2); \quad V = \frac{\lambda_{beat}}{T_{beat}} = \frac{1}{2} (v_1 + v_2)$$

Their speeds are calculated as

$$v_1 \approx 6200 \text{ (m/s)} \quad (\approx \text{observed in Evershed flow})$$

$$v_2 = \omega r_{middle} = 2017 \text{ (m/s)} \quad (\text{solar rotation}); \quad (23)$$

Where, regarding Evershed flow as the eruption of the top-layer flow, about 6km/s speed was reported [31]. Alternatively, the top-layer speed  $v_1$  also can be calculated in terms of thermodynamics, to be  $v_1=6244$  (m/s) [28]. Here using  $v_1=6100$  (m/s), their beat period  $T_{beat}$  is calculated to be a very remarkable value of 10.93 (years), in agreement with the sunspot cycle value (say, mean 11 years).

$$T_{beat} \approx \frac{4\pi c^3}{\beta(v_1^2 - v_2^2)} = 10.93 \text{ (years)} \quad (24)$$

The relative error to the mean 11 years is 0.6% for the beat period calculation using the acceleration-roll waves. This beat phenomenon turns out to be a [nucleon density oscillation](#) that undergoes to drive the sunspot cycle evolution. The beat wavelength  $\lambda_{beat}$  is too long to observe, only the beat period is easy to be observed. As shown in Fig.8, on the solar surface, the equatorial circumference  $2\pi r$  only occupies a little part of the beat wavelength, what we see is the expansion and contraction of the nucleon density.

$$\frac{2\pi r}{\lambda_{beat}} = 0.0031 \quad (25)$$

This nucleon density oscillation is understood as [a new type of nuclear reaction](#) on an astronomic scale.

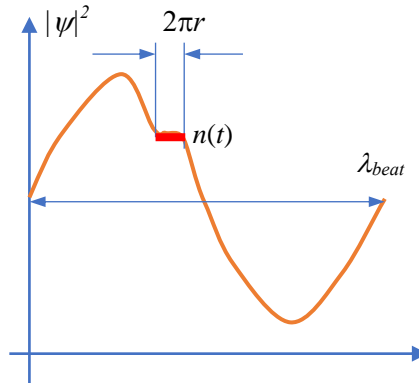


Fig.8 The equatorial circumference  $2\pi r$  only occupies a little part of the beat wavelength, what we see is the expansion and contraction of the nucleon density.

In the above calculation, although this seems to be a rough model, there is an obvious

correlation between solar radius, solar rotation, solar density, ultimate acceleration, and Planck-constant-like constant  $h$ .

## 7. Atmospheric circulation

Consider an acceleration-roll wave  $\psi_A$  in the earth shell at the latitude angle  $A$ , it will interfere with its neighbor waves within its coherent width. Because the earth shell mainly consists of dense matter, their mutual cascade-interference will cause the acceleration roll wave to have the same phase at the same longitude, so that the acceleration roll wave  $\psi_A$  should equal to the  $\psi_{equator}$  at the same longitude, as shown in Fig.9(a). This conclusion is supported by the spherical symmetry of the earth's density distribution, that is.

$$\text{spherical symmetry: } \rho(r, A, \varphi) = \rho(r) \Rightarrow \psi(r, A, \varphi) = \psi(r) \quad (26)$$

$$\text{or: } \psi_A = \psi_{equator}$$

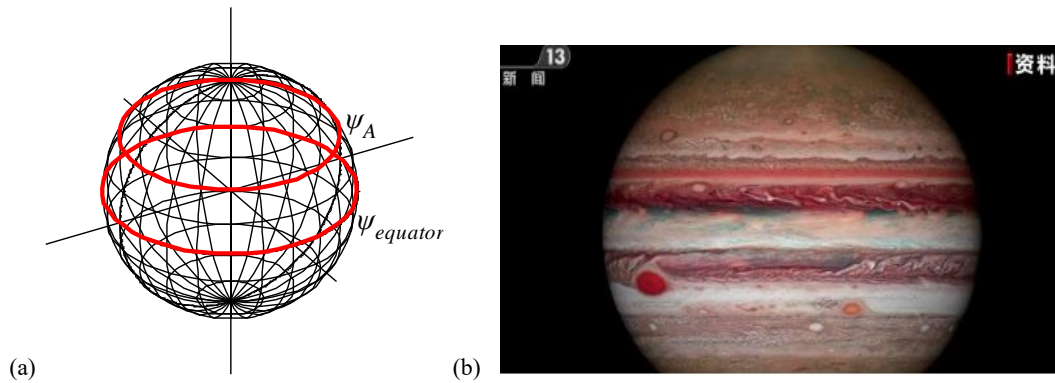


Fig.9 (a) Mutual cascade-interference will lead to the symmetry of the earth's density distribution. (b) Jupiter (the photo from News).

```
<Clet2020 Script>// [26]
double dP[20],D[2000], r, v1,v2,K1,K2; int i,j,k,N;
int main(){SetViewAngle("temp0,theta60,phi-60");
DrawFrame(FRAME_LINE,1,0xfffaf);Overlook("2,1,60",D);
for(i=0;i<180;i+=15){k=0;K1=0;K2=i;Grid();}
for(i=0;i<180;i+=15){k=1;K1=i;K2=0;Grid();}
SetPen(3,0xff0000);k=1;K1=60;K2=0;Grid();K1=90;K2=0;Grid();
//SetPen(3,0xf4ff);k=1;K1=55;K2=0;Grid();K1=65;K2=0;Grid();
TextHang(40,40,50,"#ifψ#sdA#t");TextHang(50,40,0,"#ifψ#sdequator#t");
}
Grid(){N=50;K1*=PI/180;K2*=PI/180;r=60;
if(k=0){v1=2*PI/N;v2=0;}else{v1=0;v2=2*PI/N;}
for(j=0;j<=N;j+=1){k=j+j;
D[k]=r*sin(K1)*cos(K2);D[k+1]=r*sin(K1)*sin(K2);D[k+2]=r*cos(K1);
K1+=v1;K2+=v2;}Plot("POLYGON,0,50,XYZ,10",D);
}#v07=?>A#t
```

On the contrary, in the thin atmosphere, the cascade-interference within coherence width can be ignored, so the wind and clouds are widely distributed in the sky on a large scale.

Through the coherent width concept, considering the interference between the air  $\psi_A$  at the latitude angle  $A$  and the shell  $\psi_{shell}$  at the same latitude, they are

$$\psi(r, A) = \psi_{air}(r, A) + C\psi_{shell}(r, A) = \psi_{air}(r, A) + C\psi_{shell\_equator}(r)$$

$$T_{beat} \approx \frac{4\pi c^3}{\beta(v_{shell\_equator}^2 - v_{air}^2)} \quad (27)$$

$$v_{shell\_equator} = \omega r$$

$$v_{air} = \omega r \cos(A) + v_{wind} + v_{sun\_effect}$$

where  $C$  represents the coupling constant which relates to their distance and mass fractions, their interference leads to a beat phenomenon. Positive wind represents the direction from west to east. The air is subjected to the solar radiation which enforces the beat oscillation to run at the period  $T_{beat}=1$  (year) at the latitude angles  $A=-23.5^\circ N \sim 23.5^\circ N$  due to the tilt of the earth axis with respect to the earth's orbital plane. We have known that there is a beat  $T_{beat}=1$  year in the first constructive interference ridge with zero wind at the latitude  $A_1$ , using the above neat period formula we obtain the sun effect:

$$v_{sun\_effect} = 369.788 - \omega r \cos(A_1); \quad (units : m/s) \quad (28)$$

Near the ridge, the sun effect is modified as

$$v_{sun\_effect} = 369.788 \cos(A - A_1) - \omega r \cos(A) \quad (29)$$

It is not easy to maintain the constructive interference condition for these waves. When the first ridge is at latitude  $A_1=12^\circ N$ , the wind required for maintaining the beat  $T_{beat}=1$  (year) near the latitude  $A=12^\circ N$  is calculated as shown in Fig.10(a) (blue line), this wind will be destroyed by destructive interference at higher latitudes. But, the wind will arise up again at the next locations where the waves satisfy the constructive interference condition: at  $A=39^\circ N$  location where beat  $T_{beat}=0.5$  (years), and at  $A=57^\circ N$  location where beat  $T_{beat}=0.37$  (years) which is the shortest period that the earth can get within the arctic regions.

$$v_{wind} = \sqrt{\omega^2 r^2 - \frac{4\pi c^3}{\beta T_{beat}}} - \omega r \cos(A) - v_{sun\_effect} \quad (30)$$

The maximal wind appears most probably at the midpoint of the first two ridges, about 48m/s. Linking all characteristic points in Fig.10(a) we obtain the predicted wind-curve over the northern hemisphere; this prediction agrees well with the experimental observations at an altitude of 10km (200hPa), as shown in Fig.11.

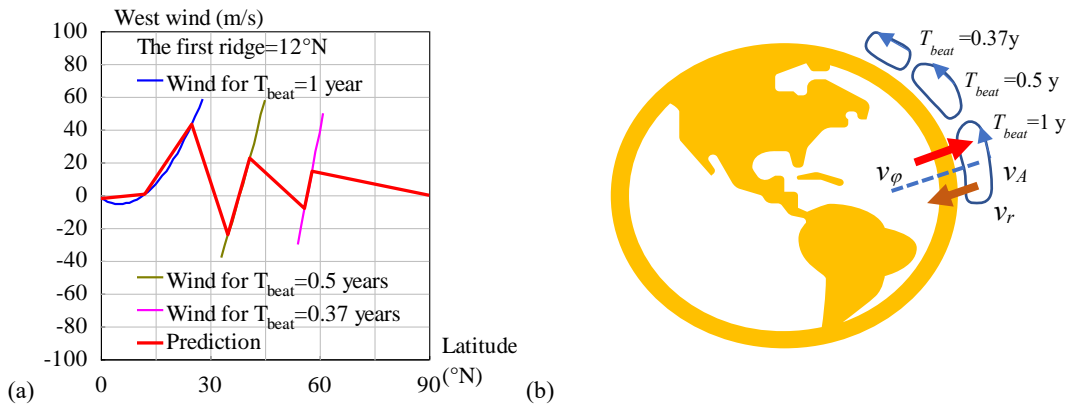


Fig.10 (a) Calculation of west winds in the northern hemisphere. (b) The atmospheric circulation in the northern

hemisphere.

```

<Clet2020 Script> [26]
double beta,H,M,r,rc,rs,rot,v1,v2,Year,T,Lamda,V,a,b,w,Fmax,N[500],S[500],F[100]; int i,j,k,t,m,n,s,f,Type,x;
int main(){beta=1.377075e+14;H=SPEEDC*SPEEDC*SPEEDC/beta;
M=5.97237e24;rs=6.371e6;rot=2*PI/(24*3600);Year=24*3600*365.2422;
Type=1; x=10; if(Type>1) x=-30;//v2=rs*rot; a=v2*v2-4*PI*H/Year; V=sqrt(a)-v2;
if(Type==1) SetAxis(X_AXIS,0,0,90,"Latitude#n(°N);0;30;60;90");
else SetAxis(X_AXIS,-90,-90,90,"Latitude#n(°N);-90;-60;-30;0;30;60;90");
SetAxis(Y_AXIS,-100,-100,100,"West wind (m/s):-100;-80;-60;-40;-20;0;20;40;60;80;100");
DrawFrame(0x016a,Type,0xaffaf);//Polyline(2,"-90,0,90,0");
Check(15,k); if(k>24) k=24; if(k<-24) k=-24; //TextAt(100,10,"V=%f",V);
T=Year/2; Wind(); f=0; Findf(); t=N[m+m]; T=Year; Wind(); f=0; Findf();
SetPen(2,0xfff); Polyline(n,N,x,70,"Wind for T#sdbeat#t=1 year"); if(Type>1) Polyline(s,S);
F[0]=N[0];F[1]=N[1]; F[2]=N[m+m]; F[3]=N[m+m+1]; t=(t+F[2])/2;//midst of two ridges
t=F[2]+m; Fmax=N[t+t+1]; //TextAt(100,20,"t=%d, Fmax=%f",t,Fmax);
f=Fmax; Findf(); F[4]=N[m+m]; F[5]=N[m+m+1];
T=Year/2; Wind(); f=Fmax/2; Findf(); t=m;f=Fmax/2; Findf();
SetPen(2,0x80ff00); Polyline(n,N,x,-50,"Wind for T#sdbeat#t=0.5 years"); if(Type>1) Polyline(s,S);
F[6]=N[t+t]; F[7]=N[t+t+1]; F[8]=N[m+m]; F[9]=N[m+m+1];
T=0.37*Year; Wind(); f=Fmax/4; Findf(); t=m;f=Fmax/4; Findf();
SetPen(2,0x9933fa); Polyline(n,N,x,-70,"Wind for T#sdbeat#t=0.37 years"); if(Type>1) Polyline(s,S);
F[10]=N[t+t]; F[11]=N[t+t+1]; F[12]=N[m+m]; F[13]=N[m+m+1]; F[14]=90; F[15]=0;
//Draw("ELLIPSE,0,2,XYX,10","15,20,25,35");TextHang(5,40,0,"a route");
SetPen(3,0xff0000); Polyline(8,F,x,-90,"Prediction"); TextHang(x,90,0,"The first ridge=%d°N", k);
}
Wind(){n=0;s=0;
for(i=0;i<90;i+=1) { a=i*PI/180; b=(i-k)*PI/180; v1=rot*rs*cos(a); v2=rot*rs;
w=369.788*cos(b)-v2*cos(k*PI/180); a=v2*v2-4*PI*H/T; V=sqrt(a)-v1-w;
if(V>-40 && V<60) {N[n+n]=i; N[n+n+1]=V; n+=1;}}
for(i=0;i<90;i+=1) { a=-i*PI/180; b=(-i-k)*PI/180; v1=rot*rs*cos(a); v2=rot*rs;
w=369.788*cos(b)-v2*cos(k*PI/180); a=v2*v2-4*PI*H/T; V=sqrt(a)-v1-w;
if(V>-40 && V<60) {S[s+s]=i; S[s+s+1]=V; s+=1;}}
Findf(){a=1e10; for(i=0;i<n;i+=1) { b=N[i+1]-f;if(b<0) b=-b;if(b<a) {m=i;a=b;}}
} //if(k==12) ClipJob(APPEND,"i=%d,V=%f",i,V);
#v07=?>A

```

For further improvement of precision, the value of the wind required by the constructive interference condition should be understood as a magnitude, it should be resolved into three components in the spherical coordinates  $(r, A, \varphi)$  as

$$v_{wind}^2 = v_r^2 + v_A^2 + v_\varphi^2 \quad (31)$$

According to the energy equipartition theorem in thermodynamics, approximately we have the average estimation

$$\langle v_r^2 \rangle = \langle v_A^2 \rangle = \langle v_\varphi^2 \rangle = \frac{1}{3} v_{wind}^2 \quad (32)$$

Thus, the wind vectors around the northern hemisphere of the Earth are plotted in Fig.10(b), the atmospheric circulation consists of three cells: Hadley cell, Ferrel cell, and arctic cell.

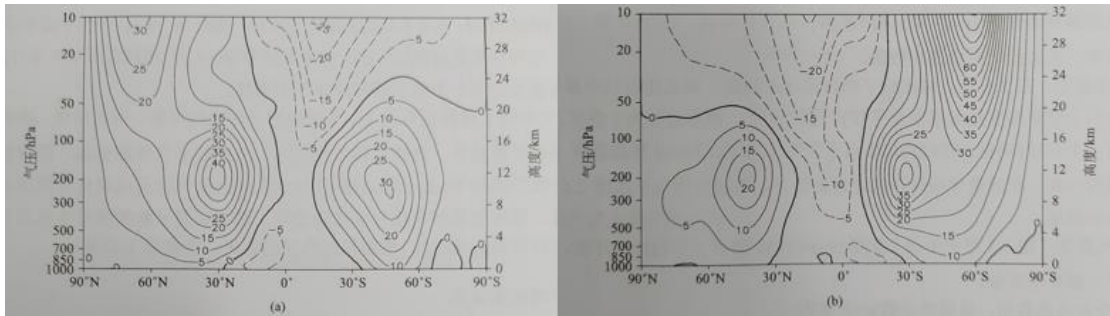


Fig.11 NCEP/NCAR data, mean west winds over 40 years (1958-1997) [36]. (a) in winter; (b) in summer.

The beat  $T_{beat}=0.5$  (years) blows comfortable winds over Europe, Northern America and Northeastern Asia, and modulates the four seasons; the shortest beat  $T_{beat}=0.37$  (years) has a beat wavelength too long to be confined in the arctic regions so that it escapes from the north pole toward the equator, so recognized as the planetary scale waves or Rossby waves.

Since the acceleration-roll wave of the air interferes with the acceleration-roll wave of the earth shell, the easterlies at the equator have a magnitude of about 10 m/s. The trade winds or easterlies are the permanent east-to-west prevailing winds that flow in the Earth's equatorial region. The trade winds blow mainly from the northeast in the Northern Hemisphere and the southeast in the Southern Hemisphere, strengthening during the winter and when the Arctic oscillation is in its warm phase. Trade winds have been used by captains of sailing ships to cross the world's oceans for centuries. The driving force of atmospheric circulation is the uneven distribution of solar heating across the earth, which is greatest near the equator and least at the poles. This air rises to the tropopause, about 10–15 kilometers above sea level, where the air is no longer buoyant [33].

Consider a funny issue, as we have known that  $v_{sun\_effect} = -84(\text{m/s})$  at the equator when the first ridge at  $A_1=12^\circ\text{N}$ , imagine if nuclear wars happen on the earth to stop the solar radiation to the earth's surface, then the equatorial wind on the earth's surface will simply reach to  $-94(\text{m/s})$ , like the winds on the surfaces of Jupiter and Saturn [28], this will change global climate mode, killed all dinosaurs by strong winds and dusts. Thinking about Mars, Jupiter, and Saturn that gain very weak solar radiation, and there are at least 100 (m/s) strong winds on their surfaces, as shown in Fig.9(b). This section helps us understand how the dinosaurs to be buried.

## 8. North pole generates cold streams per 2.24 years

In the fact, the primary acceleration-roll wave  $\phi$  at the third ridge vicinity is in a situation of destructive interference, it must wrap the arctic regions loosely for surviving so that  $|\phi|^2 \neq 0$ , as illustrated in Fig.12(a); otherwise, if it wraps tightly, then destructive interference condition will kill it completely until  $|\phi|^2 = 0$  everywhere. Winds just play a role to loosen the wrapping process. In practice, only beats of primary acceleration-roll waves are visible.

In the preceding section, we have mentioned that the third beat  $T_{beat} = 0.37(\text{years})$  is the shortest period that the earth can get within the arctic regions because of

$$v_{air} = \sqrt{\omega^2 r^2 - \frac{4\pi c^3}{\beta T_{beat}}} > 0 \Rightarrow T_{beat} \geq 0.37(\text{years}) . \quad (33)$$

It covers the whole arctic. Apparently, the third beat does not satisfy orbital closeness for adapting to solar radiation cycle (1 year), actually a closed orbit should be

$$T_{beat} = \frac{1}{3}(\text{years}) = 0.3333(\text{years}) . \quad (34)$$

which undergoes a 1:3 resonant relationship with the solar radiation cycle. Hence, the third beat  $\psi_{3rd}$  cannot be tightly confined in the arctic regions, it would split into two components:

$$\psi_{3rd} = \psi_{0.3333y} + \psi_{stream} . \quad (35)$$

In the arctic regions the third beat  $\psi_{3rd}$  would contain the closed  $\psi_{0.3333y}$  while generate cold streams  $\psi_{stream}$  expelled into their surroundings, as shown in Fig.12(b). The beat  $\psi_{3rd}$  is slower than  $\psi_{0.3333y}$ , so that the cold streams  $\psi_{stream}$  leave  $\psi_{0.3333y}$  as easterlies initially, gently these flows become southeast winds because the arctic regions refuse them. The expelled cold streams  $\psi_{stream}$  toward equatorial zone is recognized as Rossby waves which were discovered in 1966 by Yanai and Maruyama [42].

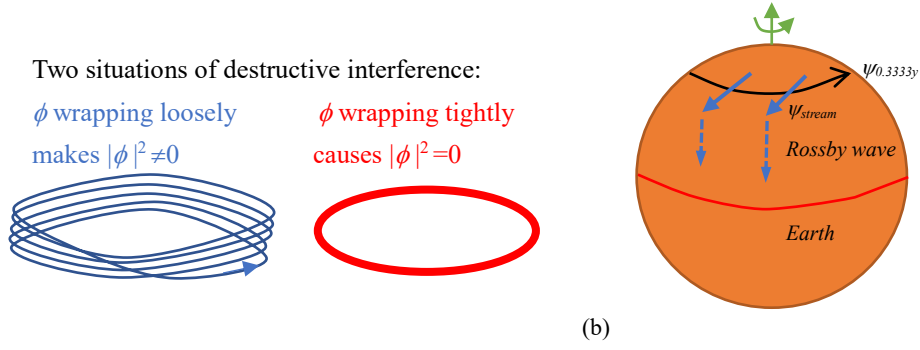


Fig.12 (a)  $\phi$  wraps loosely or tightly. (b) The third beat  $\psi_{3rd}$  would contain the  $\psi_{0.3333y}$  while generate cold streams  $\psi_{stream}$ .

The interference between the third beat  $\psi_{3rd}$  and the closed beat  $\psi_{0.3333y}$  gives out the scattering cold streams

$$|\psi_{stream}|^2 = |\psi_{3rd} - \psi_{0.3333y}|^2 = 2 - 2 \cos\left(\frac{-2\pi l}{\lambda_{stream}} - \frac{2\pi t}{T_{stream}}\right) . \quad (36)$$

and the period formula

$$\frac{1}{T_{stream}} = \frac{1}{T_{0.3333y}} - \frac{1}{T_{0.37y}} . \quad (37)$$

The cold streams initially go down as easterlies across the west wind zone between the third ridge and second ridge, finally arrive at the equatorial zone and become oscillating winds in the southeast mode or southwest mode alternatively. The 70--10 hPa monthly mean zonal wind data are shown in Fig.13, observed at Singapore in Asia [43], which indicates that the cold streams reach equatorial vicinity with an oscillating period of  $T_{stream}=2.24$ (years). We have to correct the third ridge's beat by the period  $T_{beat}=0.3916$ (years) instead of the previous  $T_{beat}=0.37$ (years), thus theoretical prediction is just  $T_{stream} = 2.24$ (years), which agrees with the observed cycles of the quasi-biennial oscillation in the equatorial lower stratosphere in Fig.13.

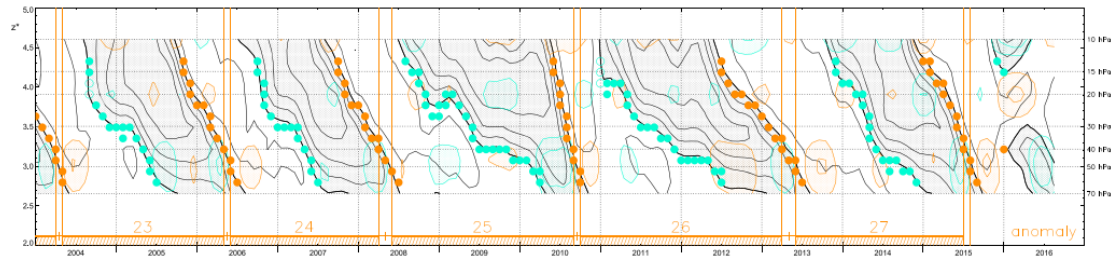


Fig.13 Time-height cross section of monthly mean zonal wind in recent years, from Singapore rawinsonde data, 70--10 hPa, interpolated to 15 equally spaced levels in log pressure. Easterlies are shaded, and the contour interval is 10 m/s. Superposed on the figure are zero crossings identified in vertical profiles of interpolated data. The solid circles indicate that vertical shear and temporal acceleration are of the same sign, consistent with the standard model; the open circles indicate that they are opposite. The color contours and shading correspond to a partial wind anomaly constructed from the third and fourth RPCs. IDL contouring may alter details near the zero-wind line, which, from time to time, appear inconsistent with the identified zero crossings (e.g., end of 2008). In such instances the raw vertical profiles are considered more reliable than the contoured data [43].

From the previous  $T_{beat}=0.37(\text{years})$  to the present  $T_{beat}=0.3916(\text{years})$  in the arctic regions, we accepted a relative error of 5.5% for the present theory to predict the cycle of 2.24 years.

The cold streams leaving arctic regions must have a speed that is strong enough to swim bravely across the west wind zone between the third ridge and second ridge at 200hPa altitude (10km), go along with the Hadley cell and Ferrel cell in atmospheric circulations [42], finally arrive at the equatorial zone with a speed that is strong enough to cope with the equatorial easterlies at 200hPa altitude (10km). Therefore, we estimate that the cold streams leaving arctic regions must have a speed of 20m/s, and have a speed of 10m/s at the equatorial zone. It does not mean that the cold streams will collide with the west winds directly, because their main streams may flow at different altitudes in the sky, their strengths should be of the same order of magnitude. The cold streams go down toward the south as scattering waves, dissipates themselves off in the journey.

The closed beat  $\psi_{0.3333y}$  only has vague pattern in the arctic atmosphere due to many other disturbances and other dissipations. Comparing to the earth's circumference, the wavelength of a beat is given by

$$\begin{aligned} T_{beat} &= 1 \text{ year}; & \frac{2\pi r}{\lambda_{beat}} &= 0.003 \\ T_{beat} &= 0.5 \text{ years}; & \frac{2\pi r}{\lambda_{beat}} &= 0.007 \\ T_{beat} &= 0.3916 \text{ years}; & \frac{2\pi r}{\lambda_{beat}} &= 0.01 \end{aligned} \quad (38)$$

```
<Clet2020 Script> [26]
double beta,H,M,r,rc, rs, rot,v1,v2, Year,T,Lamda,V,a,b,w;
int main(){beta=1.377075e+14; H=SPEEDC*SPEEDC*SPEEDC/beta;
M=5.97237e24; rs=6.378e6; rot=2*PI/(24*3600); Year=24*3600*365.2422;T=0.3916;
v2=rs*rot; a=v2*v2-4*PI*H/(T*Year); v1=sqrt(a);V=(v2+v1)/2; Lamda=V*T*Year;w=2*PI*rs/Lamda;
TextAt(100,20,"v1=%f, v2=%f, V=%f, #nT=%f, Lamda=%e, w=%f",v1,v2,V, T, Lamda,w);
}#v07=?>A
```

So that we cannot get the view of waveform of these beats on the earth surface, as illustrated in Fig.8, what we can see is the nucleon density  $|\psi|^2$  variation as time varies on an astronomic scale.

The cold streams per 2.24 years is a quantum fluid behavior, its strength and clock were synchronized with the earth's quantum system, which cannot be settled by traditional fluid mechanics, for spin and superfluidity like superconductivity, see Ref. [28].

## 9. European climate pattern

European continent locates at latitudes from about 35°N to 70°N, there is a west wind of 25m/s at the altitude 10km above the continent, with some weaker easterlies, it contains the second and third constructive interference ridges in its sky, as shown in Fig.14.

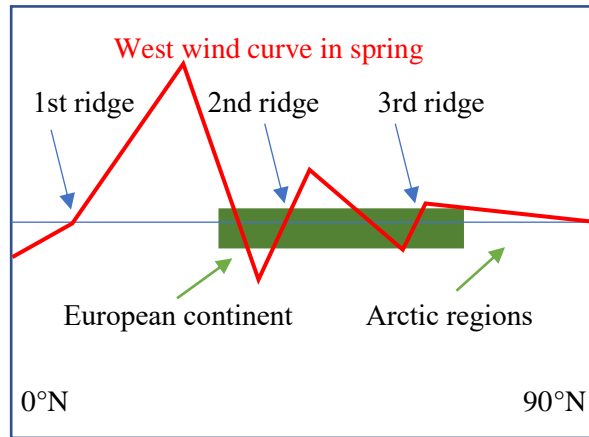


Fig.14 The constructive interference ridges at the altitude 10km on northern hemisphere in spring.

The two ridges swing over the Europe in accordance with season change due to the tilt of the earth's axis, Europe also suffers to a gust of cold streams from arctic regions per 2.24 years. The European climate pattern is under control of the second ridge's beat  $T_{beat}=0.5$  years and the third ridge's cold streams per 2.24 years.

(1) The second ridge's beat  $T_{beat}=0.5$  years modulates out four seasons for the Europe.

Most of Europe is located in the north temperate zone, with a mild and humid climate. The western Atlantic coast is cool in summer, mild in winter, and rainy and foggy. It is a typical marine temperate broad-leaved forest climate. The east belongs to continental temperate broad-leaved forest climate because it is far from the sea. The northern part of the Eastern European Plain has a temperate coniferous forest climate. The Arctic Ocean coastal areas are cold in winter and cool and short in summer, belonging to the cold tundra climate. The southern Mediterranean coastal area is warm and rainy in winter, hot and dry in summer, with a subtropical Mediterranean climate.

(2) West wind zone blows vapors from Atlantic Ocean to the European continent.

Cyclones in Western Europe are active frequently, with more precipitation. The annual precipitation in the west of the British Isles is more than 1000 mm, and that in the west coast of Scotland can reach 2000 mm or more. In other areas, it is between 600 and 1000 mm. The seasonal distribution of precipitation is relatively uniform, with a little more in autumn and winter in the west and a little more in summer in the east. For example, Dublin accounts for 26% in autumn and winter respectively, and 24% in spring and summer respectively; Cologne accounts for 31% in summer, 25% in autumn, 23% in winter and 21% in spring.

(3) The third ridge's cold streams invade the European continent per 2.24 years

When Mongolia's high-pressure force is very strong and the polar continental air mass in the east invades, it often leads to disastrous cold weather. Northern part of the European Plain, the latitude is high, the winter is long, the summer is short and cool. Under the control of polar ocean air mass, the climate of the western coast of Scandinavia is marine all year round. The temperature in winter is about  $0^{\circ}\text{C}$ , and the precipitation is abundant. From the east of the Scandinavian Mountains to Ural, the role of polar continental air mass and ice ocean air mass increases. The climate transition is continental, and the winter is cold. The temperature drops gradually from west to east. The average temperature in January  $-4.4^{\circ}\text{C}$  to  $-15.4^{\circ}\text{C}$ . When the

ice ocean air mass intrudes, it often appears  $-30^{\circ}\text{C}$  and  $-40^{\circ}\text{C}$  severe cold. It is generally cool in summer. The average temperature in July is  $10-12^{\circ}\text{C}$  in the north and  $16-18^{\circ}\text{C}$  in the south. The growth period is not long, generally 3-4 months. The duration of growth temperature (above  $10^{\circ}\text{C}$ ) suitable for rye, flax and vegetables in Eastern Europe is only 90 days at most, so agriculture here is underdeveloped.

(4) The Global Climate Change:  $+0.8^{\circ}\text{C}$  for the Past Century, see viXra:2208.0123, 2022.

(5) Study of Earthquakes Using Quantum Gravity Theory, see viXra:2209.0149, 2022.

(6) Calculation of Cyclones Using Quantum Gravity Theory, see viXra:2209.0139, 2022.

(7) Smart hunters can quickly find rabbits, deer or foxes by tracking animals in the snow. As we have known, wind is required to meet the conditions of constructive interference, therefore, the appearance of a gust is the signal of a quantum system which works in the atmosphere. Extracting energy from winds and rivers actually sabotages the quantum stability of the Earth's atmosphere, which may inevitably change the global climate, as shown in Fig.15.

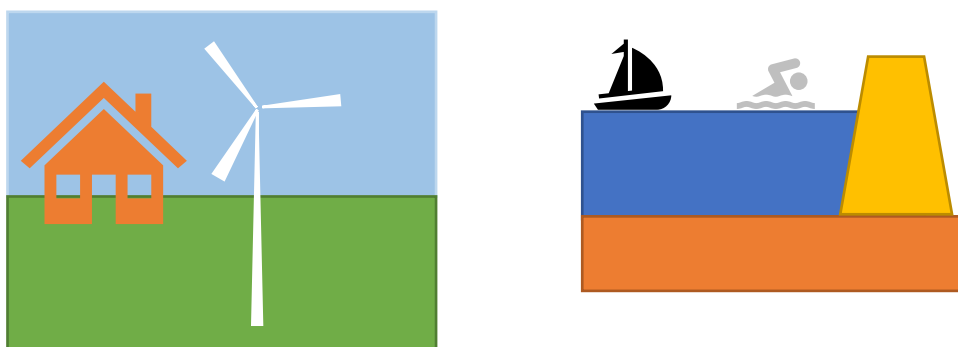


Fig.15 Extracting energies from winds and rives actually sabotages the quantum stability of the earth's atmosphere, may inevitably change the global climate.

## 10. Conclusions

In analogy with the ultimate speed  $c$ , there is an ultimate acceleration  $\beta$ , nobody's acceleration can exceed this limit  $\beta$ , in the solar system,  $\beta=2.961520e+10(\text{m/s}^2)$ . Because this ultimate acceleration is large, any effect related to  $\beta$  will become easy to test, including quantum gravity tests. In this paper, an approach is put forward to connect the ultimate acceleration with quantum theory, therefore the ultimate acceleration has quantum effects. At the first, this approach is applied to sunspot problems, the sunspot cycle is calculated to be 10.93 years. Next, this approach is applied to the atmospheric circulations and European climate pattern. Constructive interference condition takes place at three latitudes on the northern hemisphere, that control overall wind fields around the earth. This quantum effect indicates that Europe suffers to a gust of cold streams from arctic regions per 2.24 years, this prediction agrees well with the observed cycles of the quasi-biennial oscillation in the equatorial lower stratosphere. The European climate pattern is under control of the four seasons and the cold streams per 2.24 years.

## References

- [1]C. Marletto, and V. Vedral, Gravitationally Induced Entanglement between Two Massive Particles is Sufficient Evidence of Quantum Effects in Gravity, Phys. Rev. Lett., 119, 240402 (2017)  
 [2]T. Guerreiro, Quantum effects in gravity waves, Classical and Quantum Gravity, 37 (2020) 155001 (13pp).

- [3]S. Carlip, D. Chiou, W. Ni, R. Woodard, Quantum Gravity: A Brief History of Ideas and Some Prospects, *International Journal of Modern Physics D*, V,24,14,2015,1530028. DOI:10.1142/S0218271815300281.
- [4]de Broglie, L., *CRAS*,175(1922):811-813, translated in 2012 by H. C. Shen in *Selected works of de Broglie*.
- [5]de Broglie, Waves and quanta, *Nature*, 112, 2815(1923): 540.
- [6]de Broglie, Recherches sur la théorie des Quanta, translated in 2004 by A. F. Kracklauer as De Broglie, Louis, *On the Theory of Quanta*. 1925.
- [7]NASA, <https://solarscience.msfc.nasa.gov/interior.shtml>.
- [8]NASA, <https://nssdc.gsfc.nasa.gov/planetary/factsheet/marsfact.html>.
- [9]B. Ryden *Introduction to Cosmology*, Cambridge University Press, 2019, 2nd edition.
- [10]D. Valencia, D. D. Sasselov, R. J. O'Connell, Radius and structure models of the first super-earth planet, *The Astrophysical Journal*, 656:545-551, 2007, February 10.
- [11]D. Valencia, D. D. Sasselov, R. J. O'Connell, Detailed models of super-earths: how well can we infer bulk properties? *The Astrophysical Journal*, 665:1413-1420, 2007 August 20.
- [12]T. Guillot, A. P. Showman, Evolution of "51Pegasus-like" planets, *Astronomy & Astrophysics*, 2002, 385, 156-165, DOI: 10.1051/0004-6361:20011624
- [13]T. Guillot, A. P. Showman, Atmospheric circulation and tides of "51Pegasus-like" planets, *Astronomy & Astrophysics*, 2002, 385, 166-180, DOI: 10.1051/0004-6361:20020101
- [14]L.N. Fletcher, Y. Kaspi, T. Guillot, A.P. Showman, How Well Do We Understand the Belt/Zone Circulation of Giant Planet Atmospheres? *Space Sci Rev*, 2020, 216:30. <https://doi.org/10.1007/s11214-019-0631-9>
- [15]Y. Kaspi, E. Galanti, A.P. Showman, D. J. Stevenson, T. Guillot, L. Iess, S.J. Bolton, Comparison of the Deep Atmospheric Dynamics of Jupiter and Saturn in Light of the Juno and Cassini Gravity Measurements, *Space Sci Rev*, 2020, 216:84. <https://doi.org/10.1007/s11214-020-00705-7>
- [16]Orbital Debris Program Office, *HISTORY OF ON-ORBIT SATELLITE FRAGMENTATIONS*, National Aeronautics and Space Administration, 2018, 15 th Edition.
- [17]M. Mulrooney, The NASA Liquid Mirror Telescope, *Orbital Debris Quarterly News*, 2007, April, v11i2,
- [18]Orbital Debris Program Office, Chinese Anti-satellite Test Creates Most Severe Orbital Debris Cloud in History, *Orbital Debris Quarterly News*, 2007, April, v11i2,
- [19]A. MANIS, M. MATNEY, A. VAVRIN, D. GATES, J. SEAGO, P. ANZ-MEADOR, Comparison of the NASA ORDEM 3.1 and ESA MASTER-8 Models, *Orbital Debris Quarterly News*, 2021, Sept, v25i3.
- [20]D. Wright, Space debris, *Physics today*, 2007, 10, 35-40.
- [21]TANG Zhi-mei, DING Zong-hua, DAI Lian-dong, WU Jian, XU Zheng-wen, "The Statistics Analysis of Space Debris in Beam Parking Model in 78° North Latitude Regions," *Space Debris Research*, 2017, 17, 3, 1-7.
- [22]TANG Zhimei DING, Zonghua, YANG Song, DAI Liandong, XU Zhengwen, WU Jian The statistics analysis of space debris in beam parking model based on the Arctic 500 MHz incoherent scattering radar, *CHINESE JOURNAL OF RADIO SCIENCE*, 2018, 25, 5, 537-542
- [23]TANG Zhimei, DING, Zonghua, DAI Liandong, WU Jian, XU Zhengwen, Comparative analysis of space debris gaze detection based on the two incoherent scattering radars located at 69N and 78N, *Chin . J . Space Sci*, 2018 38, 1, 73-78. DOI:10.11728/cjss2018.01.073
- [24]DING Zong-hua, YANG Song, JIANG hai, DAI Lian-dong, TANG Zhi-mei, XU Zheng-wen, WU Jian, The Data Analysis of the Space Debris Observation by the Qujing Incoherent Scatter Radar, *Space Debris Research*, 2018, 18, 1, 12-19.
- [25]YANG Song, DING Zonghua, Xu Zhengwen, WU Jian, Statistical analysis on the space posture, distribution, and scattering characteristic of debris by incoherent scattering radar in Qujing, *Chinese Journal of Radio science*, 2018 33, 6 648-654, DOI:10.13443/j.cjors.2017112301
- [26]Clet Lab, Clet: a C compiler, <https://drive.google.com/file/d/1OjKqANcgZ-9V56rgcoMtOu9w4rP49sgN/view?usp=sharing>
- [27]Huaiyang Cui, Relativistic Matter Wave and Its Explanation to Superconductivity: Based on the Equality Principle, *Modern Physics*, 10, 3(2020)35-52. <https://doi.org/10.12677/MP.2020.103005>
- [28]Huaiyang Cui, Relativistic Matter Wave and Quantum Computer, Amazon Kindle eBook, 2021.
- [29]Huaiyang Cui, Ultimate Acceleration to Calculate Atomic Spin, *viXra:2209.0041*, 2022.
- [30]Huaiyang Cui, Study of Earthquakes in Japanese Islands Using Quantum Gravity Theory with Ultimate Acceleration, *viXra:2209.0149*, 2022.
- [31]N.Cox, *Allen's Astrophysical Quantities*, Springer-Verlag, 2001, 4th ed..
- [32] S. E. Schneider, T. T. Arny, *Pathways to Astronomy*, McGraw-Hill Education, 2018, 5th ed.
- [33] [https://en.wikipedia.org/wiki/E1\\_Ni%C3%B1o%E2%80%93Southern\\_Oscillation](https://en.wikipedia.org/wiki/E1_Ni%C3%B1o%E2%80%93Southern_Oscillation)
- [34] [https://en.wikipedia.org/wiki/Atmosphere\\_of\\_Earth](https://en.wikipedia.org/wiki/Atmosphere_of_Earth)
- [35] Y.M.Zhu, et al, *Principle of Meteorology*, China meteorology Press, 2019. p.243.
- [36] Liping Li et al, *Introduction to Atmospheric Circulation*, 2nd edition, Science Press, 2021,
- [37] [https://en.wikipedia.org/wiki/Tropical\\_cyclone](https://en.wikipedia.org/wiki/Tropical_cyclone)
- [38] [https://en.wikipedia.org/wiki/Tropical\\_cyclone\\_basins](https://en.wikipedia.org/wiki/Tropical_cyclone_basins)
- [39] <https://en.wikipedia.org/wiki/pulsar>.
- [40] L A. Lyne and F. Graham-Smith, *Pulsar Astronomy*, Fourth Edition, Cambridge University Press, 2012.
- [41] Ian Morison, *Introduction to Astronomy and Cosmology*, John Wiley & Sons, 2008.
- [42] J.R.Holton, G.J.Hakim, *An Introduction to Dynamic Meteorology*, fifth ver., 2013, Elsevier Inc.
- [43] T.J.Dunkerton, Nearly identical cycles of the quasi-biennial oscillation in the equatorial lower stratosphere, *Journal of Geophysical Research: Atmosphere*, 122, 8467-8493, (2017). Doi: 10.1002/2017JD026542.